RESEARCH PAPER

The pyrenoidal linker protein EPYC1 phase separates with hybrid Arabidopsis–Chlamydomonas Rubisco through interactions with the algal Rubisco small subunit

Nicky Atkinson[1], Christos N. Velanis[1], Tobias Wunder[2], David J. Clarke[3], Oliver Mueller-Cajar[2] and Alistair J. McCormick[1,*,]

[1] SynthSys and Institute of Molecular Plant Sciences, School of Biological Sciences, University of Edinburgh, Edinburgh EH9 3BF, UK
[2] School of Biological Sciences, Nanyang Technological University, 60 Nanyang Drive, Singapore 637551, Singapore
[3] School of Chemistry, University of Edinburgh, Edinburgh EH9 3FJ, UK

* Correspondence: alistair.mccormick@ed.ac.uk

Abstract

Photosynthetic efficiencies in plants are restricted by the CO_2-fixing enzyme Rubisco but could be enhanced by introducing a CO_2-concentrating mechanism (CCM) from green algae, such as *Chlamydomonas reinhardtii* (hereafter Chlamydomonas). A key feature of the algal CCM is aggregation of Rubisco in the pyrenoid, a liquid-like organelle in the chloroplast. Here we have used a yeast two-hybrid system and higher plants to investigate the protein–protein interaction between Rubisco and essential pyrenoid component 1 (EPYC1), a linker protein required for Rubisco aggregation. We showed that EPYC1 interacts with the small subunit of Rubisco (SSU) from Chlamydomonas and that EPYC1 has at least five SSU interaction sites. Interaction is crucially dependent on the two surface-exposed α-helices of the Chlamydomonas SSU. EPYC1 could be localized to the chloroplast in higher plants and was not detrimental to growth when expressed stably in Arabidopsis with or without a Chlamydomonas SSU. Although EPYC1 interacted with Rubisco *in planta*, EPYC1 was a target for proteolytic degradation. Plants expressing EPYC1 did not show obvious evidence of Rubisco aggregation. Nevertheless, hybrid Arabidopsis Rubisco containing the Chlamydomonas SSU could phase separate into liquid droplets with purified EPYC1 *in vitro*, providing the first evidence of pyrenoid-like aggregation for Rubisco derived from a higher plant.

Keywords: *Arabidopsis thaliana*, *Chlamydomonas reinhardtii*, chloroplast, CO_2-concentrating mechanism, *Nicotiana benthamiana*, photosynthesis, pyrenoid.

Introduction

Meeting the food demands of the rising global population is one of the most pressing challenges for plant science (Long *et al.*, 2015; Simkin *et al.*, 2019). The required increases are un-likely to be achieved entirely through traditional crop breeding approaches or agricultural land expansion, and agricultural sectors are increasingly looking to new genome engineering approaches for solutions (Borel *et al.*, 2017; Waltz *et al.*, 2017). Improving photosynthetic conversion efficiencies is a prom-ising strategy to achieve this goal, and several recent examples in crops have demonstrated the capacity for photosynthetic enhancements in crop species using this approach (Kromdijk *et al.*, 2016; Driever *et al.*, 2017; Lopez-Calcagno *et al.*, 2019).

Much research is focused on overcoming the limitations of C_3 photosynthesis, which is the most common form of CO_2 assimilation in plants, including critical staple crops (e.g. rice, wheat, and soybean) (Simkin *et al*., 2019). In C_3 plants, delivery of carbon dioxide (CO_2) to chloroplasts occurs by passive diffusion, which limits photosynthetic efficiencies. A further limitation is imposed by the unfavourable catalytic properties of the primary carboxylase enzyme, Rubisco, located in the chloroplasts of leaf cells (Bathellier *et al*., 2018). Rubisco restricts CO_2 assimilation in plants because it has a slow turnover rate and a relatively low affinity for CO_2—it is only half-saturated with CO_2 at concentrations inside C_3 chloroplasts. To compensate, C_3 plants invest up to 25% of leaf nitrogen into producing Rubisco (Parry *et al*., 2013). Rubisco also catalyses a competitive side reaction with oxygen (O_2) that typically leads to substantial metabolic costs associated with a salvage process for the oxygenated product, called photorespiration (Busch *et al*., 2018). Photorespiration can result in a loss of productivity of up to 50% in C_3 plants (South *et al*., 2018).

Several photosynthetic organisms, including cyanobacteria, algae, and a group of land plants called hornworts, have evolved biophysical CO_2–concentrating mechanisms (CCMs) that actively increase the CO_2 concentration around Rubisco. Researchers are currently working towards the introduction of these CCMs into C_3 plants to increase the carboxylation efficiency of Rubisco and reduce photorespiration (Rae *et al*., 2017; Long *et al*., 2018). Engineering a biophysical CCM into higher plants is predicted to significantly enhance photosynthetic rates and productivity (Price *et al*., 2013; McGrath and Long, 2014; Yin and Struik, 2017). The eukaryotic algal CCM is composed of inorganic carbon (Ci) transporters at the plasma membrane and chloroplast envelope, which work together to deliver above ambient concentrations of CO_2 to Rubisco within a chloroplastic microcompartment called the pyrenoid (Yamano *et al*., 2015; Mackinder *et al*., 2017; Zhan *et al*., 2018). Theoretical modelling approaches have demonstrated the requirement for a pyrenoid in algal systems (Badger *et al*., 1998) and shown that some form of microcompartment containing Rubisco would also be needed for a successful CCM in higher plant systems (Price *et al*., 2013).

The algal CCM is an attractive target for transfer as key components of the CCM localize appropriately in higher plants (Atkinson *et al*., 2016). Furthermore, the Rubisco small subunit (SSU; encoded by the *rbcS* nuclear gene family) of *Chlamydomonas reinhardtii* (hereafter Chlamydomonas) can complement severely SSU-deficient Arabidopsis mutants (Atkinson *et al*., 2017), with only small impacts on Rubisco function and assembly, and plant growth close to wild-type levels reported. In contrast, the replacement of tobacco Rubisco with cyanobacterial Rubisco produced poorer growing transplastomic plants, even when grown at greatly elevated CO_2 concentrations, due to the low affinity of cyanobacterial Rubisco for CO_2 and its low level of expression (Lin *et al*., 2014; Occhialini *et al*., 2016; Long *et al*., 2018). Thus, the challenges of introducing an algal-based CCM incorporating appropriate structural modifications that enable Rubisco aggregation might be readily testable without large perturbations to plant growth or a requirement for high CO_2.

Recent work in Chlamydomonas has revealed new details about the structure and composition of the pyrenoid as a highly dynamic organelle with liquid-like properties rather than a static solid or crystalline structure (Engel *et al*., 2015; Freeman Rosenzweig *et al*., 2017; Mackinder *et al*., 2017). When the CCM is active, the pyrenoid matrix is composed primarily of Rubisco, Rubisco activase, and essential pyrenoid component 1 (EPYC1), a Rubisco linker protein important for Rubisco packaging in the pyrenoid (Mackinder *et al*., 2016). EPYC1 is an intrinsically disordered protein containing four repeated regions that are predicted to bind Rubisco via multiple low affinity interactions to promote phase transitions, which in turn allow dynamic internal rearrangement within the pyrenoid consistent with its liquid-like organization (Hyman *et al*., 2014; Freeman Rosenzweig *et al*., 2017; Yizhi *et al*., 2018). Pyrenoid formation is also dependent on the amino acid composition of the Rubisco SSU and, more specifically, on two surface-exposed α-helices, which differ markedly between Chlamydomonas and higher plants (Meyer *et al*., 2012). Recent work has shown that Rubisco from Chlamydomonas and EPYC1 are necessary and sufficient to induce the liquid–liquid phase separation observed in pyrenoids and that such interactions with EPYC1 are strongly influenced by the presence of the Chlamydomonas SSU (Wunder *et al*., 2018). Currently little is known regarding the potential interactive binding sites between EPYC1 and Rubisco.

Here we reveal new insights into the protein–protein interaction between EPYC1 and Rubisco through their expression in two heterologous systems: yeast and higher plants. When expressed *in planta*, EPYC1 appeared unstable. However, hybrid Rubisco complexes from Arabidopsis were able to phase separate with purified EPYC1 *in vitro*, thus recapitulating the liquid-like behaviour of the Chlamydomonas pyrenoid. We discuss the implications of these findings for ongoing efforts to introduce a functional algal CCM into a higher plant.

Materials and methods

Plant material and growth conditions

Arabidopsis (*Arabidopsis thaliana*, Col-0) seeds were sown on compost, stratified for 3 d at 4 °C, and grown at 20 °C, ambient CO_2, 70% relative humidity, and 150 μmol photons m^{-2} s^{-1} in 12 h light, 12 h dark. For comparisons of different genotypes, plants were grown from seeds of the same age and storage history, harvested from plants grown in the same environmental conditions. *Nicotiana benthamiana* (L.) was grown at 20 °C with 150 μmol photons m^{-2} s^{-1} in 12 h light, 12 h dark.

Construct design and transformation

The coding sequence of EPYC1 was codon optimized for expression in higher plants using an online tool (www.idtdna.com/CodonOpt). All variants of EPYC1 were synthesized as Gblock fragments (IDT) and cloned directly into level 0 acceptor vectors (pAGM1299 and pICH41264) of the Plant MoClo system (Engler *et al*., 2014) or pB7WG2,0 vectors containing C- or N-terminal yellow fluorescent protein (YFP; Supplementary Table S1 at *JXB* online). To generate fusion proteins, gene expression constructs were assembled into binary level M acceptor vectors. Level M vectors were transformed into *Agrobacterium tumefaciens* (AGL1) for transient gene expression in *N. benthamiana* (Schöb *et al*., 1997) or stable insertion in Arabidopsis

plants by floral dipping (Clough and Bent, 1998). Homozygous insertion lines were identified in the T_3 generation using the pFAST-R selection cassette (Shimada *et al*., 2010).

DNA and leaf protein analyses

PCRs were performed as in McCormick and Kruger (2015) using gene-specific primers (Supplementary Table S2). Soluble protein was extracted from frozen leaf material of 21-d-old plants (sixth and seventh leaf) in 5× Bolt LDS sample buffer (ThermoFisher Scientific) with 200 mM DTT at 70 °C for 15 min. Extracts were centrifuged and the supernatants subjected to SDS–PAGE on a 4–12% (w/v) polyacrylamide gel and transferred to a nitrocellulose membrane. Membranes were probed with rabbit serum raised against wheat Rubisco at 1:10 000 dilution (Howe *et al*., 1982) or against EPYC1 at 1:2000 dilution (Mackinder *et al*., 2016), followed by horseradish peroxidase (HRP)-linked goat anti-rabbit IgG (Abcam) at 1:10 000 dilution, and visualized using Pierce ECL Western Blotting Substrate (Life Technologies).

Growth analysis and photosynthetic measurements

Rosette growth rates were quantified using an in-house imaging system (Dobrescu *et al*., 2017). Maximum quantum yield of PSII (F_v/F_m) was measured using a Hansatech Handy PEA continuous excitation chlorophyll fluorimeter (Hansatech Instruments Ltd). (Maxwell and Johnson, 2000).

Co-immunoprecipitation (co-IP)

Rosettes of 35-day-old Arabidopsis plants expressing EPYC1 in a complemented Rubisco mutant background (S2$_{Cr}$, 1A$_{At}$MOD, or 1A$_{At}$) were snap-frozen and ground in liquid N_2. An equal volume of IP extraction buffer [100 mM HEPES (pH 7.5), 150 mM NaCl, 4 mM EDTA, 5 mM DTT, 0.4 mM phenylmethylsulfonyl fluoride (PMSF), 10% (v/v) glycerol, 0.1% (v/v) Triton X-100, and one Roche cOmplete EDTA-free protease inhibitor tablet per 10 ml] was added, samples were rotated at 4 °C for 15 min, centrifuged at 4 °C, and filtered through two layers of Miracloth (Merck). Each extract (2 ml) was pre-cleared by incubating with 50 μl of Protein A Dynabeads (ThermoFisher Scientific) pre-equilibrated in IP buffer for 1 h at 4 °C, before discarding the beads. Antibody-coated beads were generated by applying 3.5 μg of anti-EPYC1 antibody to 50 μl of Protein A Dynabeads, which were then rotated at 4 °C for 30 min. The antibody was cross-linked to the beads using Pierce BS^3 cross-linking agent (Thermo Scientific). Each protein extract was incubated with the antibody-coated beads and rotated at 4 °C for 2 h. Unbound sample (flow-through) was discarded and the beads were washed four times with washing buffer [20 mM Tris–HCl (pH 8), 150 mM NaCl, 0.1% (w/v) SDS, 1% (v/v) Triton X-100, 2 mM EDTA]. Immunocomplexes were eluted by adding 50 μl of elution buffer (2× LDS sample buffer, 200 mM DTT) and heating for 15 min at 70 °C, before discarding beads and subjecting to SDS–PAGE and immunoblotting.

Immunogold labelling and electron microscopy

Leaf samples were taken from 21-day-old S2$_{Cr}$ and S2$_{Cr}$_EPYC1 plants and fixed with with 4% (v/v) paraformaldehyde, 0.5% (v/v) glutaraldehyde, and 0.05 M sodium cacodylate (pH 7.2). Leaf strips (1 mm wide) were vacuum infiltrated with fixative three times for 15 min, then rotated overnight at 4 °C. Samples were rinsed three times with phosphate-buffered saline (PBS) then dehydrated sequentially by vacuum infiltrating with 50, 70, 80, and 90% ethanol (v/v) for 1 h each, then three times with 100%. Samples were infiltrated with increasing concentrations of LR White Resin [30, 50, and 70% (w/v)] mixed with ethanol for 1 h each, then with 100% resin three times. The resin was polymerized in capsules at 50 °C overnight. Sections (1 μm thick) were cut on a Leica Ultracut ultramicrotome, stained with Toluidine Blue, and viewed with a light microscope to select suitable areas for investigation. Ultrathin sections (60 nm thick) were cut from selected areas and mounted onto plastic-coated copper grids. Grids were blocked with 1% (w/v) BSA in TBSTT [Tris–buffered saline with 0.05% (v/v) Triton X-100 and 0.05% (v/v) Tween-20], incubated overnight with anti-Rubisco antibody in TBSTT at 1:250 dilution, and washed twice with TBSTT and water. Incubation with 15 nm gold particle-conjugated goat anti-rabbit secondary antibody (Abcam) in TBSTT was carried out for 1 h at 1:200 dilution, before washing as before. Grids were stained in 2% (w/v) uranyl acetate then viewed in a JEOL JEM–1400 Plus transmission electron microscope. Images were collected on a GATAN OneView camera.

Confocal laser scanning microscopy

Leaves were imaged with a Leica TCS SP2 laser scanning confocal microscope (Leica) as in Atkinson *et al*. (2016).

Protein production, droplet sedimentation assay, and microscopy

Rubisco was purified from 25- to 30-day-old Arabidopsis rosettes using a combination of ammonium sulfate precipitation, ion-exchange chromatography, and gel filtration (Shivhare and Mueller–Cajar, 2017). Rubisco was purified from Chlamydomonas cells (CC-2677), and EPYC1 and EPYC1::GFP (green fluorescent protein) was produced in *Escherichia coli* and purified as described in Wunder *et al*. (2018). EPYC1–Rubisco droplets reconstituted at room temperature in 10 μl reactions for 5 min in buffer A [20 mM Tris–HCl (pH 8.0), and 50 mM NaCl] were separated at 4 °C from the bulk solution by centrifugation for 4 min at 21 100 *g*. Pellet (droplet) and supernatant (bulk solution) fractions were subjected to SDS–PAGE and Coomassie staining. For light and fluorescence microscopy, reaction solutions (5 μl) were imaged after 3–5 min with a Nikon Eclipse Ti Inverted Microscope using the settings for differential interference contrast and epifluorescence microscopy (using fluorescein isothiocyanate filter settings) with a ×100 oil-immersion objective focusing on the coverslip surface. The coverslips used were 22×22 mm (Superior Marienfeld, Germany) and fixed in one-well Chamlide CMS chamber for 22×22 coverslips (Live Cell Instrument, South Korea). ImageJ was used to pseudocolour all images.

Liquid chromatography–mass spectrometry

Cell lysate was prepared from Chlamydomonas cells according to Mackinder *et al*. (2016). Following membrane solubilization with 2% (w/v) digitonin, the clarified lysate was applied to 150 μl of Protein A Dynabeads that had been incubated with 20 μg of anti-EPYC1 antibody. The Dynabead–cell lysate was incubated for 1.5 h with rotation at 4 °C. The beads were then washed four times with IP buffer [50 mM HEPES, 50 mM KOAc, 2 mM Mg(OAc)$_2$·4H$_2$O, 1 mM CaCl$_2$, 200 mM sorbitol, 1 mM NaF, 0.3 mM NA$_3$VO$_4$, Roche cOmplete EDTA-free protease inhibitor] containing 0.1% (w/v) digitonin. EPYC1 was eluted from the beads by incubating for 10 min in elution buffer [50 mM Tris–HCl, 0.2 M glycine (pH 2.6)], and the eluate was immediately neutralized with 1:10 (v/v) Tris–HCl (pH 8.5). A small amount of the eluate was run on an SDS–PAGE gel and stained with Coomassie (Supplementary Fig. S6A), and the remaining sample was used for LC-MS.

Intact protein LC-MS experiments were performed on a Synapt G2 Q-ToF instrument equipped with electrospray ionization (Waters Corp., Manchester, UK). LC separation was achieved using an Acquity UPLC equipped with a reverse phase C4 Aeris Widepore 50×2.1 mm HPLC column (Phenomenex, CA, USA), and a gradient of 5–95% acetonitrile (0.1% formic acid) over 10 min was employed. Data analysis was performed using MassLynx v4.1, and deconvolution was performed using MaxEnt.

Yeast two-hybrid (Y2H) assay

The two-hybrid plasmid vectors pGBKT7 and pGADT7 were used to detect interactions between proteins of interest. Genes were amplified using Q5 DNA polymerase (NEB) and cloned into each vector using the multiple cloning site, thus creating fusions with either the GAL4-DNA binding domain or activation domain, respectively (Supplementary Table

S1). Competent yeast cells (Y2H Gold, Clontech) were prepared from a 50 ml culture grown in YPDA medium supplemented with kanamycin (50 μg ml^{-1}). Cells were washed with ddH$_2$O and a lithium acetate/ TE solution [100 mM LiAc, 10 mM Tris–HCl (pH 7.5), 1 mM EDTA] before re-suspending in lithium acetate/TE solution. Cells were then co-transformed with binding and activation domain vectors by mixing 50 μl of competent cells with 1 μg of each plasmid vector and a poly-ethylene (PEG) solution [100 mM LiAc, 10 mM Tris–HCl (pH 7.5), 1 mM EDTA, 40% (v/v) PEG 4000]. Cells were incubated at 30 °C for 30 min, then subjected to a heat shock of 42 °C for 20 min. The cells were centrifuged, re-suspended in 500 μl of YPDA, and incubated at 30 °C for ~90 min, then centrifuged and washed in TE. The pellet was re-suspended in 200 μl of TE, spread onto SD-L-W (standard dextrose medium lacking leucine and tryptophan; Anachem), and grown for 3 d at 30 °C. Ten to fifteen of the resulting colonies were pooled per co-transformation and grown in a single culture for 24 h. The following day, 1 ml of culture was harvested, cell density (OD$_{600}$) measured, centrifuged, and then diluted in TE to give a final OD$_{600}$ of 0.5 or 0.1. Yeast cultures were then plated onto SD-L-W and SD-L-W-H (Anachem) containing different concentrations of the HIS3 inhibitor tri-aminotriazole (3-AT), and incubated for 3 d before assessing for the presence or absence of growth, as in van Nues and Beggs (2001). Protein extraction was carried out by re-suspending cells to an OD$_{600}$ of 1 from an overnight liquid culture in a lysis buffer [50 mM Tris–HCl (pH 6), 4% (v/v) SDS, 8 M urea, 30% (v/v) glycerol, 0.1 M DTT, 0.005% (w/v) Bromophenol Blue], incubating at 65 °C for 30 min, and loading directly onto a 10% (w/v) Bis-Tris protein gel (Expedeon).

Results

EPYC1 interacts with the small subunit of Rubisco

The two α-helices of the Chlamydomonas SSU have been proposed previously as potential binding sites for EPYC1 (Fig. 1A–D) (Meyer *et al.*, 2012; Mackinder *et al.*, 2016). We set out to test this hypothesis using a semi–quantitative Y2H approach. Chlamydomonas has two similar SSU homologues, S1$_{Cr}$ and S2$_{Cr}$, which are the same size, have identical α-helices and β-sheets, but differ in amino acid sequence by four residues. EPYC1 showed a relatively strong protein–protein interaction with both S1$_{Cr}$ and S2$_{Cr}$ (i.e. growth at 10 mM 3-AT) (Fig. 1E). In contrast, EPYC1 did not interact with the 1A SSU from Arabidopsis (1A$_{At}$) but did interact weakly with a hybrid 1A SSU carrying the α-helices from Chlamydomonas (1A$_{At}$MOD) (Atkinson *et al.*, 2017). The Y2H assay showed that EPYC1 does not interact with itself, other Chlamydomonas CCM components associated with the pyrenoid (i.e. LCIB, LCIC, and CAH3), or another intrinsically disordered protein found in the chloroplast stroma (AtCP12; Lopez–Calcagno *et al.*, 2014) (Supplementary Fig. S1). These results indicate that EPYC1 is not prone to false-positive protein–protein interactions in Y2H assays.

The α-helices of the SSU are critical for interaction with EPYC1

We next set out to identify the key domains on the Chlamydomonas SSU required for interaction with EPYC1. To isolate the structural components of the SSU, we generated a total of six different chimeric versions of 1A$_{At}$ bearing residues from S1$_{Cr}$ associated with the three distinct β-sheets (βA, βC, and βD), the βA–βB loop, and the two α-helices (αA

and αB) (Spreitzer, 2003) (Fig. 1C; Supplementary Fig. S2). As before, EPYC1 did not interact with 1A$_{At}$, and the addition of the β-sheets or the βA–βB loop from S1$_{Cr}$, or both together, did not permit interaction (Fig. 2; Supplementary Fig. S3A). Interactions were only observed in the presence of the two α-helices from the Chlamydomonas SSU. The α-helices alone produced a minimal interaction (i.e. on 0 mM 3-AT), which was strengthened by the incorporation of the β-sheets and the βA–βB loop from S1$_{Cr}$. Notably, the modified 1A$_{At}$ variant with the α-helices, β-sheets, and βA–βB loop from Chlamydomonas (i.e. 79% sequence identity to S1$_{Cr}$) showed a stronger interaction compared with S1$_{Cr}$, indicating that SSUs can be engineered for increased affinity for EPYC1.

EPYC1 is a modular protein, and the predicted α-helices are important for interaction with the SSU

We initially generated a variety of truncated EPYC1 variants to characterize the key regions of EPYC1 required for interaction with the SSU. EPYC1 is a modular protein consisting of four highly similar repeat sequences flanked by shorter terminal regions. Thus, truncations were made to eliminate each region sequentially from either the N- or C-terminus direction (Fig. 3A; Supplementary Figs S3B, S4). Truncated EPYC1 variants were expressed well in yeast (Supplementary Fig. S5). In Y2H experiments, the EPYC1 N-terminus alone (N-ter) did not interact with S1$_{Cr}$. Addition of the first EPYC1 repeat region was sufficient to detect interaction, and each subsequent repeat region correlated with growth at increased concentrations of 3-AT, indicating that EPYC1 is a modular protein and each repeat has an additive effect on SSU interaction. Addition of the C-terminal tail further increased the strength of the interaction. Interestingly, the C-terminus alone interacted with S1$_{Cr}$, suggesting that SSU–binding sites are not limited to the repeat regions. Removal of the N-terminus also increased the interaction strength, which is consistent with the predicted role of the N-terminus as a chloroplastic transit peptide that would be cleaved during import into the chloroplast (Mackinder *et al.*, 2016). Prediction tools ChloroP and PredAlgo suggest cleavage at residues 78 and 170, respectively (Emanuelsson *et al.*, 2007). However, both predictions are unconvincing as they would result in cleavage within the repeat regions. To identify the potential cleavage site, we immunoprecipitated and analysed EPYC1 from Chlamydomonas using electrospray ionization-MS (ESI-MS). Intact protein ESI-MS analysis revealed several proteoforms of mature EPYC1 ranging from 29 622 Da to 30 621 Da (Supplementary Fig. S6). The molecular mass difference between proteoforms was 80 Da, suggesting variable phosphorylation states; an observation consistent with previous reports highlighting the highly phosphorylated nature of EPYC1 (Turkina *et al.*, 2006; Wang *et al.*, 2014). The highly post-translationally modified state of EPYC1 made determination of the precise molecular mass of the mature protein difficult. However, the smallest proteoform identified had a molecular mass of 29.6 kDa which, based on the theoretical mass of EPYC1, indicates a cleavage site between residues 26 (V) and 27 (A) (Fig. 1B).
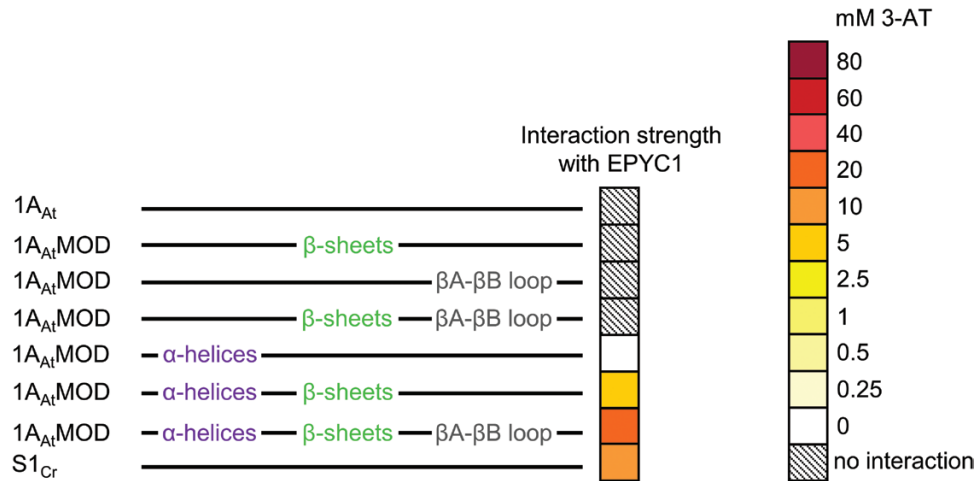
A

EPYC1

B

```
MATISSMRVGAASRVVVSGRVKTVKVAARGSWRESSTATVQASRASSATNR
VSPTRSVLPANWRQELESLRNGNGSSSAASSAPAPARSSSASWRDAAPASSSAPARSSSSASKKA
VTPSRSALPSNWKQELESLRSS__SPAPASSAPAPARSSSASWRDAAPASSSAPARSSS_SKKA
VTPSRSALPSNWKQELESLRSS__SPAPASSAPAPARSSSASWRDAAPASSSAPARSSSASKKA
VTPSRSALPSNWKQELESLRSN_SPAPASSAPAPARSSSASWRDA_PASSS___SSSA_DKA
*:*:**.**:**:**:****** .. * : ***************** ****: : *** **
GTNPWTGKSKPEIKRTALPADWRKGL
```

C

Rubisco small subunit

βA-βB loop

β-sheets

α-helices

D

```
S1_Cr  MMVWTPVNNKMFETFSYLPPLTDEQIAAQVDYIVANGW
1A_At  MQVWPPIGKKKFETLSYLPDLTDSELAKEVDYLIRNKW
       * ** *:.:* ***:**** ***.::* :***:: * *

S1_Cr  IPCLEFAEADKAYVSNESAIRFGSVSCLYYDNRYWTMW
1A_At  IPCVEFELEHG-FVY-----REHGNSPGYYDGRYWTMW
       ***:** . :* * . * ***.******

S1_Cr  KLPMFGCRDPMQVLREIVACTKAFPDAYVRLVAFDNQK
1A_At  KLPLFGCTDSAQVLKEVEECKKEYPNAFIRIIGFDNTR
       ***:*** * ***:*: *.* :*:*::*::.*** :

S1_Cr  QVQIMGFLVQRPKTARDFQPANKRSV
1A_At  QVQCISFIAYKPPSFTG---------
       *** :.*:. :* : .
```

E

Fig. 1. EPYC1 interacts with the Rubisco small subunit. (A and B) EPYC1 consists of four near identical repeat regions (highlighted in yellow, green, blue, and purple), each containing a predicted α-helix (red, underlined). The putative cleavage site of the chloroplastic transit peptide between 26 (V) and 27 (A) is indicated. The N- and C- termini are shown in grey. (C) The predicted model of the small subunit of Rubisco (SSU; 1A_At shown) has similar features in algae and higher plants, including four β-sheet (green) and two α-helical (purple) regions. (D) Amino acid alignments of mature Arabidopsis SSU 1A (1A_At) and Chlamydomonas SSU 1 (S1_Cr). Residues in red indicate the four amino acids that differ between the two Chlamydomonas SSUs, S1_Cr and S2_Cr (T/S, A/S, T/S, F/W). (E) Yeast two-hybrid interactions with EPYC1. Interaction strength is demonstrated by growth on increasing concentrations of the inhibitor 3-AT. Abbreviations: 3-AT, 3-amino-1,2,4-triazole; BD, binding domain; AD, activation domain; 1A_AtMOD, modified 1A_At carrying the two α-helical regions from Chlamydomonas; SD-L-W, yeast synthetic minimal medium (SD medium) lacking leucine (L) and tryptophan (W); SD-L-W-H, SD medium lacking L, W, and histidine (H). See Supplementary Fig. S1 for Y2H additional controls.

We hypothesized that the interaction between EPYC1 and the SSU may be mediated through a predicted α–helix conserved in each of the four repeats, which together would allow EPYC1 to bind at least four Rubisco complexes (Mackinder *et al.*, 2016; Freeman Rosenzweig *et al.*, 2017). The relative contribution of each of the four domains was analysed by eliminating the predicted α-helical structure through mutation of the residues 'RQELESL' in the first repeat and 'KQELESL' in the subsequent three repeats to seven alanines. Mutation of a single helix did not have an impact on interaction strength. However, sequentially

Fig. 2. EPYC1 requires the α-helices of the Chlamydomonas SSU for interaction. Interaction is shown between EPYC1 and modified versions of 1A$_{At}$ (top), in which different components (see Fig. 1C, D) have been switched for those from Chlamydomonas S1$_{Cr}$ (bottom). The heat map indicates interaction strength measured with yeast two-hybrid assays by the capacity for growth on increasing concentrations of 3-AT (mM). See Supplementary Fig. S2 for SSU sequences and Supplementary Fig. S3A for raw Y2H image data.
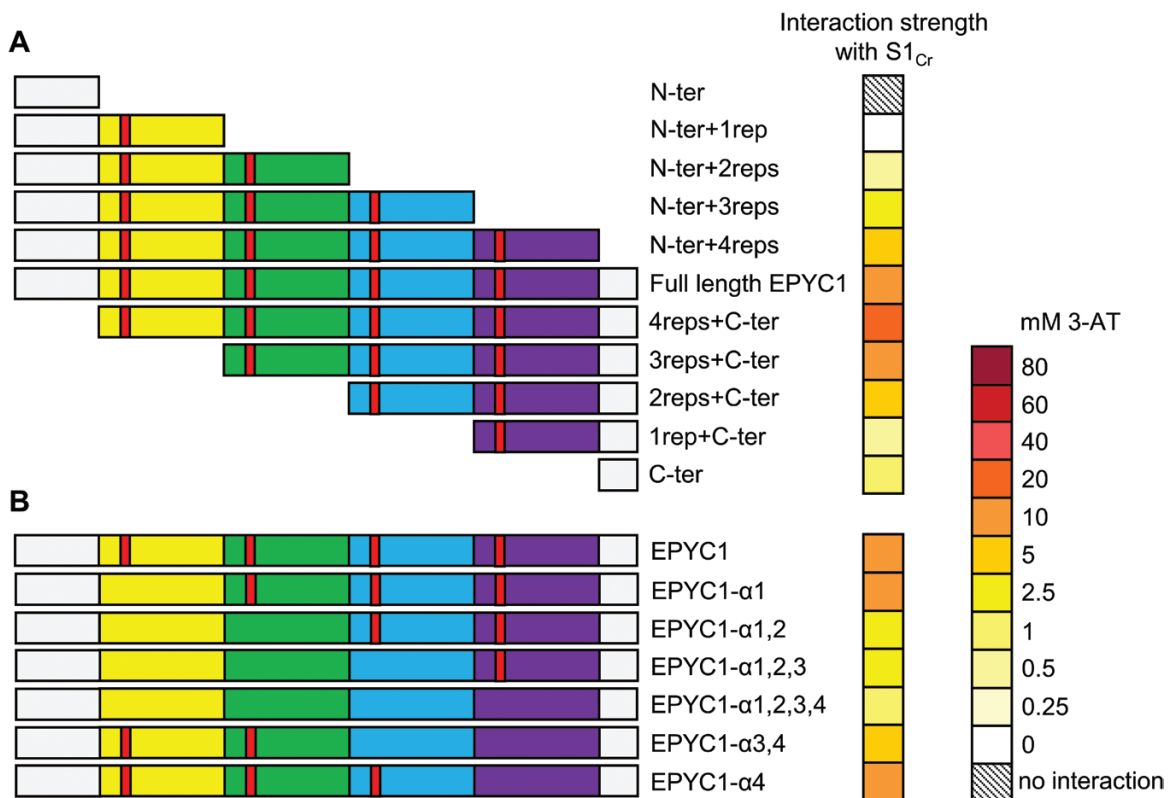
Fig. 3. EPYC1 repeat regions contribute to interaction with the Rubisco small subunit. (A) Decreasing the number of EPYC1 repeat regions reduced the strength of interaction with S1$_{Cr}$. (B) The predicted α-helical region in each repeat (red) is important for interaction with S1$_{Cr}$. These were eliminated by matutation to seven alanines in each of the different EPYC1 variants. The heat map indicates interaction strength measured with yeast two-hybrid assays by the capacity for growth on increasing concentrations of 3-AT (mM). See Supplementary Fig. S3B and C for raw Y2H image data.

weaker interactions with S1$_{Cr}$ were observed with increasing mutations of the α-helical regions (Fig. 3B; Supplementary Figs S3C, S4). If all four α-helices were mutated, the interaction was not eradicated completely. The latter finding supported our evidence for an additional SSU–binding site(s) on the C-terminus, as in the absence of all α-helices the interaction strength was reduced to the same extent as the C-terminus alone (Fig. 3A). Overall, our data suggest that EPYC1 has at least five SSU

interaction sites, located in each of its four repeat regions and the C-terminus, respectively.

EPYC1 can be modified to improve interaction strength with the SSU

Analysis of EPYC1 with PCOILS (https://toolkit.tuebingen. mpg.de/#/tools/pcoils) suggested that the putative α-helices

of EPYC1 might behave like coiled-coil domains, with the first repeat showing the highest predicted value (Fig. 4) (Gruber *et al.*, 2006; Zimmermann *et al.*, 2018). Thus, we hypothesized that the first repeat region could be a useful target scaffold to engineer a synthetic EPYC1 with increased affinity for SSU interaction. We constructed four synthetic EPYC1 variants containing one, two, four, or eight copies of the first repeat in tandem (Fig. 4A; Supplementary Fig. S3D). Four copies of the first repeat (4 rep) showed a stronger interaction strength with S1$_{Cr}$ and 1A$_{At}$MOD compared with native mature EPYC1. The strongest interaction was observed for the variant with eight repeats (8 rep), which grew on the maximum 3-AT concentrations tested (80 mM).

Using the single copy variant (1 rep), we compared modifications of the α-helix region for interaction strength based on predictions from the PCOILS tool. Duplication of the α-helical region (SVLPAN**WRQELESLRN**N**WRQEL ESLRN**GNGSS) or a G–Q substitution near the α-helix (NWRQELESLRN**Q**) predicted an increased probability of coiled-coil behaviour (Fig. 4B). In contrast to the predictions by PCOILS, the former modification eradicated the interaction, while the latter did not change the interaction strength compared with the native 1 rep variant. Finally, we attempted to knock out the interaction with either an L–R or E–W substitution within the α-helix (NWRQELESR**R**N or NWR**QW**LESLRN). Both substitutions eradicated the interaction. Our results suggest that EPYC1 α-helices do not behave like traditional coiled-coil domains, but that even single point mutations within the α-helix can affect interaction. These results support those presented in Fig. 2.
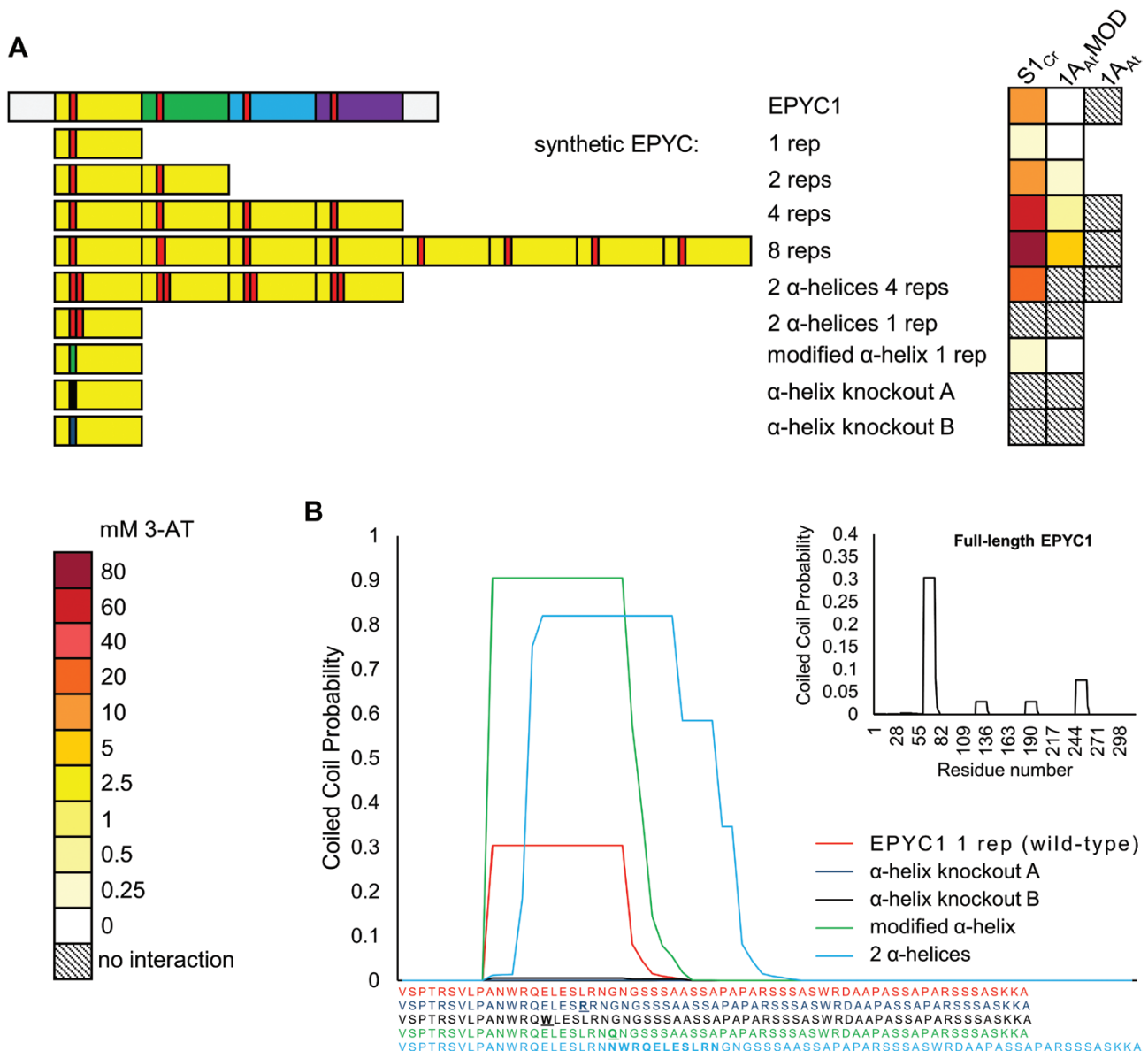
Fig. 4. EPYC1 can be modified to increase the interaction strength with SSUs. (A) Synthetic variants of EPYC1 are based on the first repeat regions (yellow) and the predicted α-helix (red). The heat map indicates interaction strength measured with yeast two-hybrid assays by the capacity for growth on increasing concentrations of 3-AT (mM). See Supplementary Fig. S3D for raw Y2H image data. (B) Predicted coiled-coil domain strengths for synthetic variants of the first repeat region of EPYC1 using the PCOILS bioinformatic tool. Matching colour-coded amino acid sequences are shown below, with residues that differ from the wild-type sequence shown in bold. The inlay shows the prediction for full-length EPYC1.

EPYC1 requires a native chloroplastic transit peptide for appropriate localization in plants

EPYC1 was codon optimized for nuclear expression in higher plants (Supplementary Fig. S7), and binary expression vectors were constructed whereby EPYC1 was C-terminally fused to GFP and expressed under the control of the 35S constitutive promoter. The localization of EPYC1::GFP was then visualized in agro-infiltrated *N. benthamiana* leaves and in stably transformed Arabidopsis plants. Unlike other chloroplast CCM components expressed in plants thus far (Atkinson *et al.*, 2016), EPYC1 was not able to localize to the chloroplast in either *N. benthamiana* or Arabidopsis, with fluorescent signals absent from the chloroplast (Fig. 5). The $1A_{At}$ chloroplastic transit peptide ($1A_{At}$-TP) was therefore added to the N-terminus of the full-length EPYC1::GFP. Preservation of the full native EPYC1 leader sequence was based on a conservative strategy to avoid removing any potential interaction sites. Furthermore, our Y2H results indicated that the presence of the N-terminus did not strongly affect interaction with the Rubisco SSU (Fig. 3). Fusion to $1A_{At}$-TP resulted in re-localization of EPYC1::GFP to the chloroplast stroma in both *N. benthamiana* and Arabidopsis.

EPYC1 is unstable in higher plants but does not affect plant growth performance

Wild-type Arabidopsis plants and two Rubisco small subunit (*1a3b*) mutant lines complemented with $S2_{Cr}$ or $1A_{At}MOD$, previously made by Atkinson *et al.* (2017) (Supplementary Fig. S2), were transformed with $1A_{At}$-TP::EPYC1 (lacking a GFP tag) (see Supplementary Fig. S7 for the plasmid map). We selected three homozygous T_3 lines from each background for further analyses (EPYC1_1–3, $S2_{Cr}$_EPYC1_1–3, and $1A_{At}MOD$_EPYC1_1–3). Immunoblots against $1A_{At}$-TP::EPYC1 in Arabidopsis produced a dominant band of ~34 kDa [slightly smaller than the mature native Chlamydomonas isoform (35 kDa)], suggesting cleavage of both $1A_{At}$-TP and a portion of the N-terminal region of EPYC1 (the antibody serum targets the C-terminus of EPYC1) (Emanuelsson *et al.*, 2007) (Fig. 6A; Supplementary Fig. S8A). Densitometry analysis showed that protein levels of EPYC1 in our highest expressing Arabidopsis lines were ~14 times lower than those in Chlamydomonas in relation to the Rubisco LSU (Supplementary Fig. S8B). Based on the reported ratio of ~1:6 for EPYC1 to Rubisco LSU in Chlamydomonas under low CO_2 (Mackinder *et al.*, 2016), the stoichiometry of EPYC1 to the Arabidopsis LSU in our transgenic line could therefore be estimated as 1:84. This ratio is also lower than the observed occurrence of between one and four EPYC1 peptides per Rubisco (i.e. eight LSUs) in phase-separated material in the *in vitro* reconstituted pyrenoidal system (Wunder *et al.*, 2018). In addition to a non-specific band at 29 kDa, several smaller bands were also evident for EPYC1 in Arabidopsis (Fig. 6A). Additional bands were not observed for EPYC1 extracted from Chlamydomonas or yeast (Supplementary Fig. S8A), suggesting that EPYC1 may be targeted by plant proteases.

Growth analyses showed a slightly reduced growth phenotype (i.e. area, FW, and DW) for some plants expressing $1A_{At}$-TP::EPYC1 compared with their corresponding segregants, but the observed decrease was not consistently significant (Fig. 6B, C). Similarly, the photosynthetic efficiency of plants expressing $1A_{At}$-TP::EPYC1 (measured by dark–adapted leaf fluorescence; F_v/F_m) was unaffected (Supplementary Table S3). Therefore, constitutive expression of EPYC1 in the chloroplast did not appear to impact plant growth under the conditions tested.

EPYC1 interacts with Rubisco in wild-type and complemented Arabidopsis SSU mutants

Having shown that specific SSUs can interact with EPYC1 in a Y2H system, we then investigated whether the interactions with Rubisco would occur *in planta* in two complemented *1a3b* mutants and wild-type plant lines expressing EPYC1 ($S2_{Cr}$_EPYC1_1, $1A_{At}MOD$_EPYC1_1, and EPYC1_1, respectively). We immunoprecipitated EPYC1 from each of these lines using anti-EPYC1 antibody attached to Protein A-coated beads, and analysed the elutes by immunoblot using antibodies against EPYC1 or Rubisco (Fig. 7). Unexpectedly, the LSU was detected in the elutes of $S2_{Cr}$_EPYC1 and $1A_{At}MOD$_EPYC1 lines, as well as the wild-type expressing EPYC1. To ensure that the observed co-IP was not a result of Rubisco promiscuity or non-specific binding onto the beads or antibodies, several negative controls were included. Rubisco was not detected in the eluate of pull-downs with anti-HA-coated beads or beads with no antibody, or in the eluate from $S2_{Cr}$ plants not transformed with EPYC1. Therefore, these results indicated that EPYC1 was able to interact with Rubisco in transformed plant lines in the absence of a Chlamydomonas or Chlamydomonas-like SSU. It was not possible to fully quantify the relative strength of the interactions due to the inherent variation in EPYC1 expression levels between the three lines tested. Nevertheless, the levels of EPYC1 eluted in the EPYC1 IP assays were similar, while the greater amounts of Rubisco eluted in the $1A_{At}MOD$_EPYC1 and $S2_{Cr}$_EPYC1 co-IP assays could suggest a stronger interaction with EPYC1 in those lines than in the wild-type background.

Bimolecular fluorescence complementation (BiFC) analysis was carried out to provide additional information about the EPYC1–Rubisco interaction *in vivo*. Three SSUs ($1A_{At}$, $S2_{Cr}$, and $1A_{At}MOD$) and EPYC1, each fused at the C-terminus to either YFP^N or YFP^C, were transiently co-expressed in *N. benthamiana* (Walter *et al.*, 2004). Consistent with immunoprecipitation results (Fig. 7), a BiFC signal for reconstituted YFP fluorescence was observed with plants co-expressing EPYC1 and each of the three SSUs, regardless of which protein was fused to YFP^N and which to YFP^C (Fig. S9). A negative control, AtCP12::YFP^C, unexpectedly produced a BiFC signal with $1AAt$::YFP^N. However this interaction may be artefactual because there was no interaction between $1AAt$::YFP^C and AtCP12::YFP^N.

Immunogold labelling revealed no aggregation of Rubisco in plants expressing EPYC1

To investigate the effect of EPYC1 on Rubisco aggregation *in planta*, we examined the localization of Rubisco in the
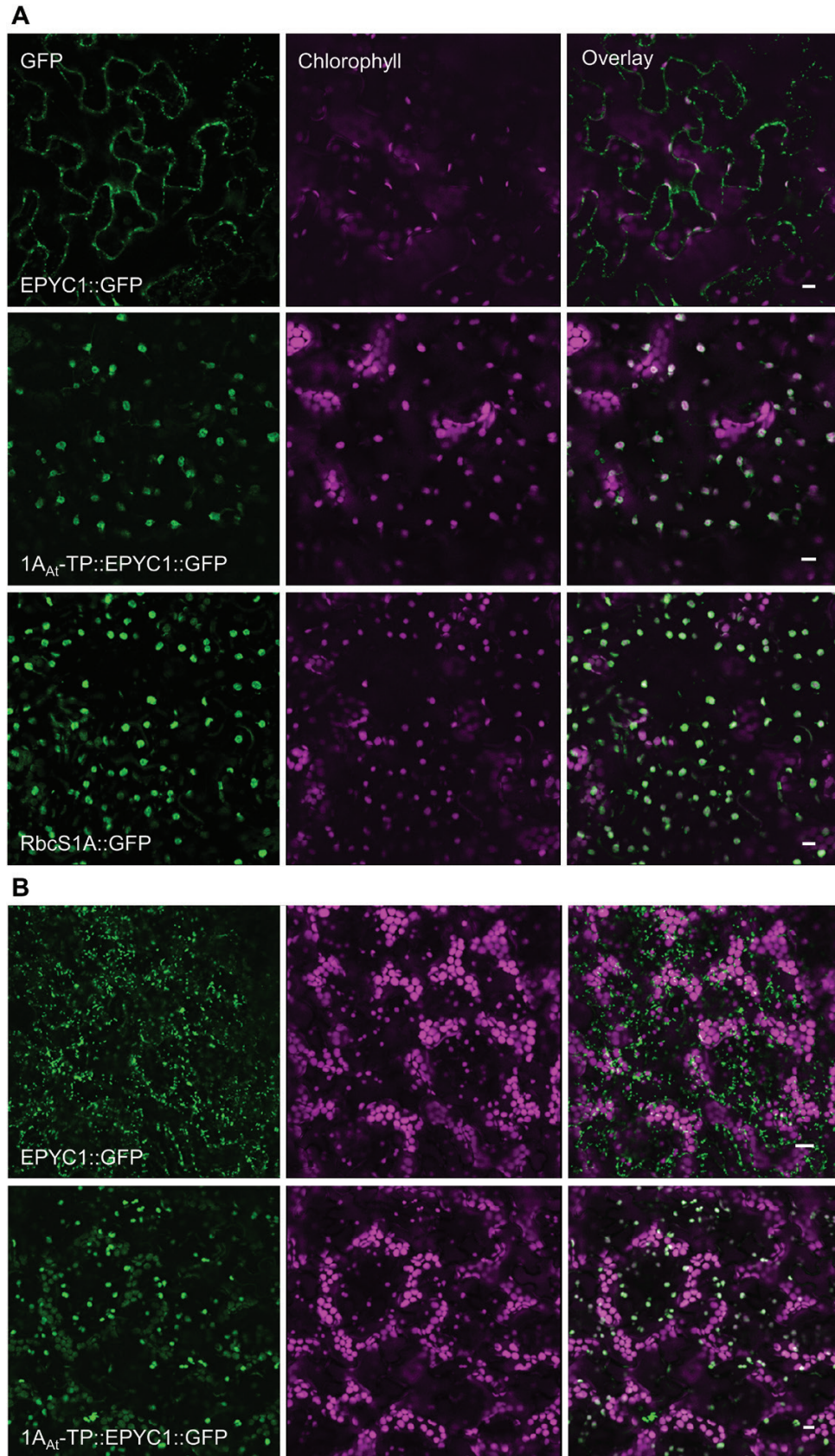
A

B

Fig. 5. Expression of GFP-fused EPYC1 with and without the 1A$_{At}$ chloroplastic transit peptide (1A$_{At}$-TP). (A) The constructs were expressed transiently in *Nicotiana benthamiana*, alongside a GFP-fused Arabidopsis 1A small subunit of Rubisco (RbcS1A::GFP). (B) Stable expression in Arabidopsis. Green and purple signals are GFP and chlorophyll autofluoresence, respectively. Overlapping signals are white. Scale bar=10 µm.
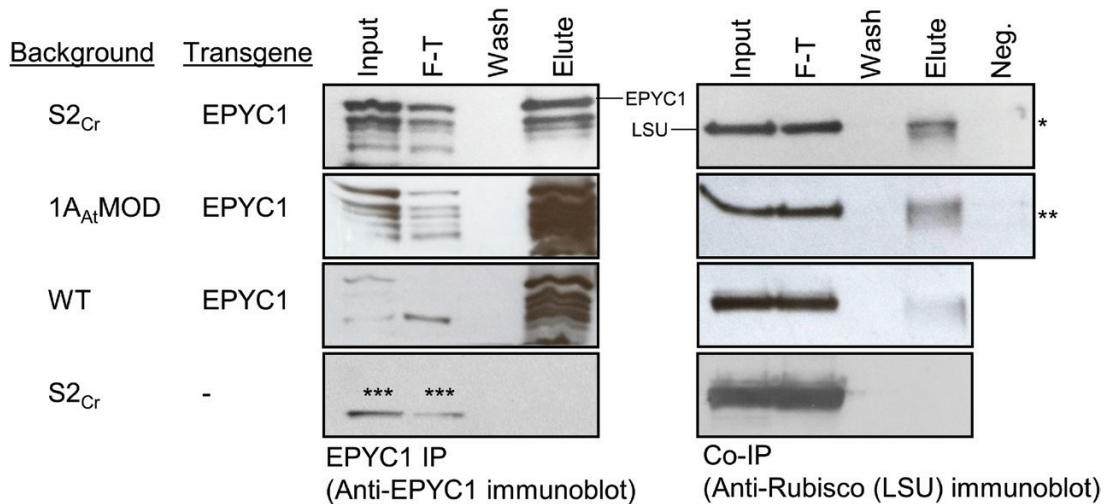
Fig. 6. Growth of Arabidopsis plant lines expressing EPYC1 fused with the $1A_{At}$-TP in either the wild-type (WT), $S2_{Cr}$, or the $1A_{At}MOD$ background. (A) Immunoblots show the relative EPYC1 expression levels in three independently transformed lines (T_3) per background, compared with their corresponding segregants (seg) lacking EPYC1. (B) Plants were harvested at 31 d, and the fresh (FW) and dry (DW) weights were measured. (C) Rosette growth of the nine transformed lines. Values are the means ±SE of measurements made on 12 (FW, DW) or 16 (growth assays) rosettes. Asterisks indicate significant difference in FW or DW between transformed lines and segregants ($P<0.05$) as determined by Student's paired sample t-tests.

Fig. 7. Co-immunoprecipitation of Rubisco with EPYC1. EPYC1 interacts with Rubisco in transgenic S2$_{Cr}$, 1A$_{At}$MOD, and wild-type (WT) lines expressing EPYC1 fused with the 1A$_{At}$-TP. Co-immunoprecipitation was performed using Protein-A coated beads that had been cross-linked to anti-EPYC1 antibody. The input, flow-through (F-T), fourth wash, and boiling elute were run on an SDS–PAGE gel, transferred to a nitrocellulose membrane, and probed with either anti-Rubisco or anti-EPYC1 antibody. Negative controls (Neg.) were carried out by replacing the anti-EPYC1 antibody on the Protein A beads with either anti-HA antibody (*) or no antibody (**) and proceeding with IP as before (only the eluted sample is shown). Asterisks (***) indicate a non-specific band observed with the anti-EPYC1 antibody in all samples including the control line not expressing EPYC1 (S2$_{Cr}$).

chloroplast of S2$_{Cr}$ complemented *1a3b* mutants expressing the highest levels of EPYC1 (S2$_{Cr}$_EPYC1_1). Immunogold label-ling of Rubisco revealed an even distribution of gold particles throughout the chloroplast when visualized by TEM similar to the S2$_{Cr}$ control not expressing EPYC1 (Supplementary Fig. S10), indicating that co-expression of EPYC1 and the Chlamydomonas SSU did not induce detectable rigid aggre-gations of Rubisco in these transformants.

EPYC1 phases separate with Rubisco from Arabidopsis SSU mutants complemented with S2$_{Cr}$

Current models of pyrenoid formation are based on specific weak multivalent interactions that promote liquid-like phase separation (Hyman *et al.*, 2014; Freeman Rosenzweig *et al.*, 2017). To observe if such interactions could occur with hybrid plant-derived Rubisco, we next examined if Rubisco from Arabidopsis *1a3b* mutants complemented with S2$_{Cr}$ was able to facilitate liquid–liquid phase separation with EPYC1 using an *in vitro* assay developed by Wunder *et al.* (2018). Rubisco was extracted from Chlamydomonas, Arabidopsis wild-type plants, and S2$_{Cr}$ lines. The hybrid Rubisco complexes in S2$_{Cr}$ lines consisted of the Arabidopsis LSU and a mixed population of Arabidopsis SSUs and S2$_{Cr}$ (~1:1) (Atkinson *et al.*, 2017). Similarly to Chlamydomonas Rubisco, hybrid plant Rubisco was able to demix with EPYC1 and formed liquid-like droplets of comparable size, albeit at slightly higher EPYC1:Rubisco ratios (Fig. 8A, B). In contrast, wild-type Arabidopsis Rubisco did not phase separate under similar conditions, indicating that the presence of S2$_{Cr}$ was critical for aggregation. In solu-tions containing Chlamydomonas or hybrid plant Rubisco, the droplets fused into a large homogeneous droplet (coalescence), supporting their liquid nature (Fig. 8C) (Hyman *et al.*, 2014). Analysis by SDS–PAGE confirmed that both EPYC1 and Rubisco had entered the droplets (Supplementary Fig. S11).

Discussion

EPYC1 is required for pyrenoid aggregation and function-ality of the CCM in Chlamydomonas and will probably be a crucial component for introducing an algal-based CCM into higher plants. Previously, EPYC1 has been shown to interact with Rubisco, but the site(s) of the interaction was unclear. Mackinder *et al.* (2016) hypothesized that interaction could be mediated through the α-helices of the SSU, as previous work had shown that exchanging the α-helices of the Chlamydomonas SSU with those from spinach inhibited pyrenoid formation (Meyer *et al.*, 2012). In addition, Wunder *et al.* (2018) have demonstrated that the Chlamydomonas SSU is important for the liquid-like aggregation typical of an algal pyrenoid. Here we have characterized this interaction by expressing EPYC1 and different SSUs together in yeast and higher plants. We have shown that the α-helical regions of the Chlamydomonas SSU are necessary and sufficient for interaction with EPYC1, and that introduction of the α-helices into an Arabidopsis SSU en-abled interaction with EPYC1. Further inclusion of additional features from the Chlamydomonas SSU strengthened the inter-action in an additive fashion, suggesting that the conformation of the SSU could have evolved, in part, to present the α-helical region to EPYC1. Although a stronger interaction may not be optimal for pyrenoid phase transitions in Chlamydomonas (Freeman Rosenzweig *et al.*, 2017), our results showed that the strength of the EPYC1–SSU interaction could be further in-creased by engineering the SSU alone. This may be required for optimizing Rubisco aggregation in higher plants while re-taining features of the higher plant SSU (Atkinson *et al.*, 2017).

We established key regions of EPYC1 that affect binding strength with the SSU. Previously Mackinder *et al.* (2016) speculated that the Rubisco-binding sites in EPYC1 were located within the four repeats. Our data supported this hy-pothesis and identified the putative α-helices in each repeat as key sites for SSU interaction. Our MS data suggested that the
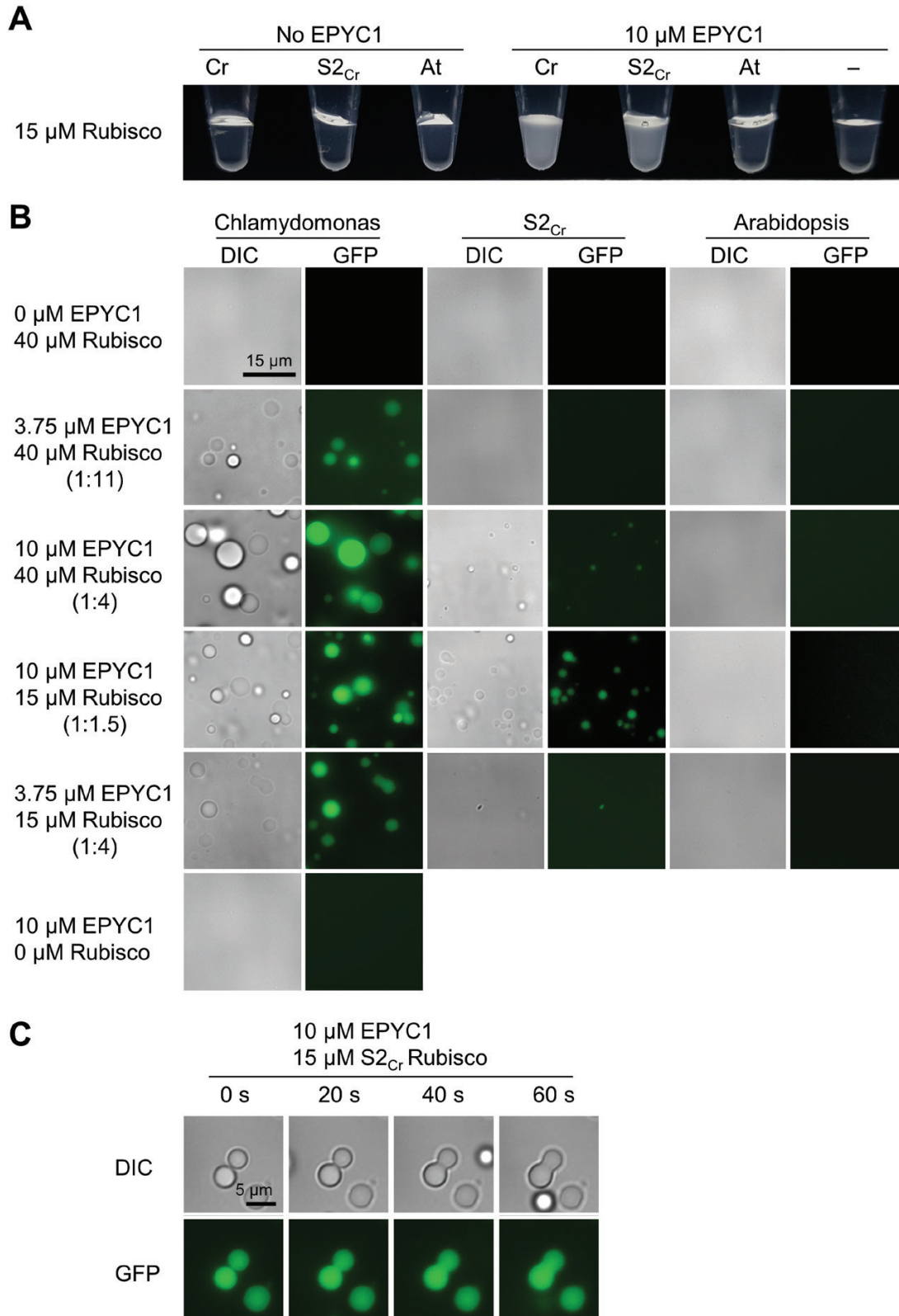
Fig. 8. Hybrid Arabidopsis Rubisco carrying a Chlamydomonas small subunit is able to phase separate and form liquid droplets with EPYC1. (A) Addition of EPYC1 to Rubisco results in turbidity in Chlamydomonas (Cr) and hybrid (S2$_{Cr}$), but not Arabidopsis (At) Rubisco (shown at ~3 min after mixing at room temperature). (B) The turbidity is caused by the formation of spherical droplets. Fluoresence in samples containing EPYC1 is due to the inclusion of EPYC1::GFP (0.25 µM). (C) Droplets from S2$_{Cr}$ Rubisco and EPYC1 fuse by coalescence. See Supplementary Fig. S11 for droplet sedimentation analysis.

N-terminus comprised a chloroplastic transit peptide (~26 res-idues in length) that is cleaved during import and maturation in Chlamydomonas (Emanuelsson *et al.*, 2007). We also showed

that the C-terminal region of EPYC1 probably contains an additional SSU interaction site(s) as this region could interact with the SSU independently as well as increase the strength of

interaction when present with the four repeats. In support of this hypothesis, Wunder *et al.* (2018) demonstrated that a single EPYC1 repeat fragment carrying the C-terminal region was sufficient to demix with Rubisco (i.e. at least two interaction sites are required to aggregate Rubisco). Based on our results, we cannot rule out the existence of additional SSU-binding sites in EPYC1. Thus, models in which EPYC1 has precisely four binding sites for Rubisco are probably too simplistic (Mackinder *et al.*, 2016). Freeman Rosenzweig *et al.* (2017) proposed a 'magic number' hypothesis, whereby the stoichiometry between the number of available EPYC1-binding sites and the surrounding Rubisco complexes defined the aggregation state of Rubisco. In their model, an odd number of binding sites was preferable for aggregation. Additional binding sites in EPYC1, for example in the C-terminal region, may help to explain such an observation. Furthermore, our data suggested that the interaction strength of EPYC1 can be modified from its native state, for example by duplicating the first repeat region. This may provide additional options for optimizing Rubisco aggregation in heterologous environments, such as higher plant chloroplasts.

Previous work has shown that most CCM components from Chlamydomonas localized to the same subcellular locations when expressed in plants (Atkinson *et al.*, 2016). Thus, we were surprised that a native chloroplastic transit peptide was required for expression of EPYC1 in higher plant chloroplasts. One explanation is that EPYC1 may be mistargeted to the mitochondrion, as chloroplast transit peptides from Chlamydomonas are known to resemble mitochondrial transit peptides in higher plants (Franzén *et al.*, 1990). Alternatively, the N-terminus might undergo proteolytic degradation when expressed in plants, thus inhibiting chloroplastic import (Doran, 2006). Even when redirected to the chloroplast with a native transit peptide, the presence on immunoblots of several smaller bands suggested that EPYC1 may be partially targeted by proteases in the chloroplast (Fig. 6; Suppleentary Fig. S8) (Nishimura *et al.*, 2017). For future work, it may be desirable to identify and modify motifs in EPYC1 recognized by native proteases to enhance EPYC1 stability, and in addition reduce the length of the native N-terminus by eliminating the sequence upstream of the putative transit peptide cleavage site (Fig. 1B).

Previous work has shown that EPYC1 can phase separate with heterologous Rubiscos of cyano- and chemoautotrophic bacterial origin (Wunder *et al.*, 2018). Even though droplet formation was less efficient for those cases, it suggests a certain promiscuity of the EPYC1–Rubisco interaction. Likewise, a residual compatibility with plant Rubisco might account for our observations made with EPYC1 expressed *in planta* (Fig. 7: Supplementary Fig. S9). EPYC1 may interact differently with free SSUs—as in yeast—and SSUs assembled into the octomeric (L8S8) Rubisco complex. Whilst no interactions with EPYC1 were evident for 1A$_{At}$ in yeast (Fig. 1), and similarly no phase separation was observed *in vitro* with wild-type Arabidopsis Rubisco and EPYC1 (Fig. 8), the high abundance of Rubisco in plant chloroplasts may increase the likelihood of potential interactions between the positively charged EPYC1 peptide and any negatively charged moieties on the LSU and/or SSU (Wunder *et al.*, 2018). Further work will be required

to distinguish whether the interactions observed *in planta* were indicative of true liquid–liquid phase separation or symptomatic of residual interactions due to the abundance of Rubisco (Hyman *et al.*, 2014)—the average concentration of Rubisco in plant chloroplasts is estimated at ~500 μM (Jensen and Bahr, 1977; Harris and Königer, 1997), which is similar to that of the pyrenoid in the Chlamydomonas chloroplast (~628 μM Rubisco) (Freeman Rosenzweig *et al.*, 2017).

Previously, Rubisco aggregates were observed in transgenic tobacco plants expressing cyanobacterial Rubisco and the β-carboxysomal assembly protein CcmM35 (Lin *et al.*, 2014). However, CcmM35 cross-links Rubisco into a highly organized and rigid paracrystalline array in β-carboxysomes (Faulkner *et al.*, 2017), which differs significantly from the dynamic and more disordered phase separation observed during the formation of pyrenoidal Rubisco aggregates mediated by EPYC1 (Engel *et al.*, 2015; Freeman Rosenzweig *et al.*, 2017; Wunder *et al.*, 2018). Promisingly, the observed interactions between EPYC1 and SSUs in yeast and recombinant EPYC1 with hybrid plant Rubisco suggest that EPYC1 does not require additional modifications or chaperones for binding. However, the low EPYC1:Rubisco protein ratio in our transgenic Arabidopsis plants, which was probably compounded by proteolytic degradation of EPYC1, was insufficient to enable detectable phase separation (Supplementary Fig. S8). Plants typically produce 4- to 5-fold more Rubisco than Chlamydomonas (30% versus 6.6% total protein per cell, respectively) (Parry *et al.*, 2013; Hammel *et al.*, 2018). Modification of EPYC1:Rubisco in the transgenic plants to give a more favourable ratio (i.e. through increased expression of EPYC1, reduction in overall Rubisco, and/or increased abundance of a pyrenoid-compatible SSU) may help to further protect EPYC1 from degradation by assembling EPYC1 with Rubisco into a pyrenoid-like structure, which might shield EPYC1 from proteases in the chloroplast. Reducing nitrogen investment in Rubisco while increasing Rubisco operating efficiency, as seen in Chlamydomonas and other photosynthetic organisms with CCMs (Rae *et al.*, 2017), is in line with our overarching goal. Such modifications could be achieved using CRISPR (clustered regularly interspaced short palindromic repeats) to target the native Arabidopsis SSU family (Pottier *et al.*, 2018; Khumsupan *et al.*, 2019). Furthermore, our data show that synthetic variants of EPYC1 could be developed to better enable aggregation of Rubisco in higher plants (Fig. 7). Recently developed tools for expressing plant Rubisco in *E. coli* offer the opportunity to more rapidly fine-tune this relationship for expression in plants going forward (Aigner *et al.*, 2017), and further explore any potential interactions between EPYC1 and other regions on the Rubisco complex. Overall, this study has demonstrated the merits of testing protein–protein interactions in different heterologous systems to improve our understanding of the algal CCM and progress current efforts to introduce a functional algal-based CCM into a higher plant.

Supplementary data

Supplementary data are available at *JXB* online.

Table S1. List of vectors used in this study.

Acknowledgements

References

Aigner H, Wilson RH, Bracher A, Calisse L, Bhat JY, Hartl FU, Hayer-Hartl M. 2017. Plant RuBisCo assembly in *E. coli* with five chloroplast chaperones including BSD2. Science **358**, 1272–1278.

Atkinson N, Feike D, Mackinder LC, Meyer MT, Griffiths H, Jonikas MC, Smith AM, McCormick AJ. 2016. Introducing an algal carbon-concentrating mechanism into higher plants: location and incorporation of key components. Plant Biotechnology Journal **14**, 1302–1315.

Atkinson N, Leitão N, Orr DJ, Meyer MT, Carmo-Silva E, Griffiths H, Smith AM, McCormick AJ. 2017. Rubisco small subunits from the unicellular green alga *Chlamydomonas* complement Rubisco-deficient mutants of Arabidopsis. New Phytologist **214**, 655–667.

Badger MR, Andrews TJ, Whitney SM, Ludwig M, Yellowlees DC, Leggat W, Price GD. 1998. The diversity and coevolution of Rubisco, plastids, pyrenoids, and chloroplast-based CO_2-concentrating mechanisms in algae. Canadian Journal of Botany **76**, 1052–1071.

Bathellier C, Tcherkez G, Lorimer GH, Farquhar GD. 2018. Rubisco is not really so bad. Plant, Cell & Environment **41**, 705–716.

Borel B. 2017. CRISPR, microbes and more are joining the war against crop killers. Nature **543**, 302–304.

Busch FA, Sage RF, Farquhar GD. 2018. Plants increase CO_2 uptake by assimilating nitrogen via the photorespiratory pathway. Nature Plants **4**, 46–54.

Clough SJ, Bent AF. 1998. Floral dip: a simplified method for *Agrobacterium*-mediated transformation of *Arabidopsis thaliana*. The Plant Journal **16**, 735–743.

Dobrescu A, Scorza LCT, Tsaftaris SA, McCormick AJ. 2017. A 'Do-It-Yourself' phenotyping system: measuring growth and morphology throughout the diel cycle in rosette shaped plants. Plant Methods **13**, 95.

Doran PM. 2006. Foreign protein degradation and instability in plants and plant tissue cultures. Trends in Biotechnology **24**, 426–432.

Driever SM, Simkin AJ, Alotaibi S, Fisk SJ, Madgwick PJ, Sparks CA, Jones HD, Lawson T, Parry MAJ, Raines CA. 2017. Increased SBPase activity improves photosynthesis and grain yield in wheat grown in greenhouse conditions. Philosophical Transactions of the Royal Society B: Biological Sciences **372**, 20160384.

Emanuelsson O, Brunak S, von Heijne G, Nielsen H. 2007. Locating proteins in the cell using TargetP, SignalP and related tools. Nature Protocols **2**, 953–971.

Engel BD, Schaffer M, Kuhn Cuellar L, Villa E, Plitzko JM, Baumeister W. 2015. Native architecture of the Chlamydomonas chloroplast revealed by in situ cryo-electron tomography. eLife **4**, e04889.

Engler C, Youles M, Gruetzner R, Ehnert TM, Werner S, Jones JD, Patron NJ, Marillonnet S. 2014. A golden gate modular cloning toolbox for plants. ACS Synthetic Biology **3**, 839–843.

Faulkner M, Rodriguez-Ramos J, Dykes GF, Owen SV, Casella S, Simpson DM, Beynon RJ, Liu LN. 2017. Direct characterization of the native structure and mechanics of cyanobacterial carboxysomes. Nanoscale **9**, 10662–10673.

Franzén LG, Rochaix JD, von Heijne G. 1990. Chloroplast transit peptides from the green alga *Chlamydomonas reinhardtii* share features with both mitochondrial and higher plant chloroplast presequences. FEBS Letters **260**, 165–168.

Freeman Rosenzweig ES, Xu B, Kuhn Cuellar L, *et al*. 2017. The eukaryotic CO_2-concentrating organelle is liquid-like and exhibits dynamic reorganization. Cell **171**, 148–162.e19.

Gruber M, Söding J, Lupas AN. 2006. Comparative analysis of coiled-coil prediction methods. Journal of Structural Biology **155**, 140–145.

Hammel A, Zimmer D, Sommer F, Mühlhaus T, Schroda M. 2018. Absolute quantification of major photosynthetic protein complexes in *Chlamydomonas reinhardtii* using quantification concatamers (QconCATs). Frontiers in Plant Science **9**, 1265.

Harris GC, Königer M. 1997. The 'high' concentrations of enzymes within the chloroplast. Photosynthesis Research **54**, 5–23.

Howe CJ, Auffret AD, Doherty A, Bowman CM, Dyer TA, Gray JC. 1982. Location and nucleotide sequence of the gene for the proton-translocating subunit of wheat chloroplast ATP synthase. Proceedings of the National Academy of Sciences, USA **79**, 6903–6907.

Hyman AA, Weber CA, Jülicher F. 2014. Liquid–liquid phase separation in biology. Annual Review of Cell and Developmental Biology **30**, 39–58.

Jensen RG, Bahr JT. 1977. Ribulose 1,5-bisphosphate carboxylase-oxygenase. Annual Review of Plant Physiology, **28**, 379–400.

Khumsupan P, Donovan S, McCormick AJ. 2019. CRISPR/Cas in Arabidopsis: overcoming challenges to accelerate improvements in crop photosynthetic efficiencies. Physiologia Plantarum **166**, 428–437.

Kromdijk J, Głowacka K, Leonelli L, Gabilly ST, Iwai M, Niyogi KK, Long SP. 2016. Improving photosynthesis and crop productivity by accelerating recovery from photoprotection. Science **354**, 857–861.

Lin MT, Occhialini A, Andralojc PJ, Parry MA, Hanson MR. 2014. A faster Rubisco with potential to increase photosynthesis in crops. Nature **513**, 547–550.

Long BM, Hee WY, Sharwood RE, *et al*. 2018. Carboxysome encapsulation of the CO_2-fixing enzyme Rubisco in tobacco chloroplasts. Nature Communications **9**, 3570.

Long SP, Marshall-Colon A, Zhu XG. 2015. Meeting the global food demand of the future by engineering crop photosynthesis and yield potential. Cell **161**, 56–66.

López-Calcagno PE, Fisk S, Brown KL, Bull SE, South PF, Raines CA. 2019. Overexpressing the H-protein of the glycine cleavage system increases biomass yield in glasshouse and field-grown transgenic tobacco plants. Plant Biotechnology Journal **17**, 141–151.

López-Calcagno PE, Howard TP, Raines CA. 2014. The CP12 protein family: a thioredoxin-mediated metabolic switch? Frontiers in Plant Science **5**, 9.

Mackinder LCM, Chen C, Leib RD, Patena W, Blum SR, Rodman M, Ramundo S, Adams CM, Jonikas MC. 2016. A repeat protein links Rubisco to form the eukaryotic carbon-concentrating organelle. Proceedings of the National Academy of Sciences, USA **113**, 5958–5963.

Mackinder LCM, Chen C, Leib RD, Patena W, Blum SR, Rodman M, Ramundo S, Adams CM, Jonikas MC. 2017. A spatial interactome reveals the protein organization of the algal CO_2-concentrating mechanism. Cell **171**, 133–147.e14.

Maxwell K, Johnson GN. 2000. Chlorophyll fluorescence—a practical guide. Journal of Experimental Botany **51**, 659–668.

McCormick AJ, Kruger NJ. 2015. Lack of fructose 2,6-bisphosphate compromises photosynthesis and growth in Arabidopsis in fluctuating environments. The Plant Journal **81**, 670–683.

McGrath JM, Long SP. 2014. Can the cyanobacterial carbon-concentrating mechanism increase photosynthesis in crop species? A theoretical analysis. Plant Physiology **164**, 2247–2261.

Meyer MT, Genkov T, Skepper JN, Jouhet J, Mitchell MC, Spreitzer RJ, Griffiths H. 2012. Rubisco small-subunit α-helices control pyrenoid formation in Chlamydomonas. Proceedings of the National Academy of Sciences, USA **109**, 19474–19479.

Nishimura K, Kato Y, Sakamoto W. 2017. Essentials of proteolytic machineries in chloroplasts. Molecular Plant **10**, 4–19.

Occhialini A, Lin MT, Andralojc PJ, Hanson MR, Parry MA. 2016. Transgenic tobacco plants with improved cyanobacterial Rubisco expression but no extra assembly factors grow at near wild-type rates if provided with elevated CO_2. The Plant Journal **85**, 148–160.

Parry MA, Andralojc PJ, Scales JC, Salvucci ME, Carmo-Silva AE, Alonso H, Whitney SM. 2013. Rubisco activity and regulation as targets for crop improvement. Journal of Experimental Botany **64**, 717–730.

Pottier M, Gilis D, Boutry M. 2018. The hidden face of rubisco. Trends in Plant Science **23**, 382–392.

Price GD, Pengelly JJ, Forster B, Du J, Whitney SM, von Caemmerer S, Badger MR, Howitt SM, Evans JR. 2013. The cyanobacterial CCM as a source of genes for improving photosynthetic CO_2 fixation in crop species. Journal of Experimental Botany **64**, 753–768.

Rae BD, Long BM, Förster B, Nguyen ND, Velanis CN, Atkinson N, Hee WY, Mukherjee B, Price GD, McCormick AJ. 2017. Progress and challenges of engineering a biophysical CO_2-concentrating mechanism into higher plants. Journal of Experimental Botany **68**, 3717–3737.

Schöb H, Kunz C, Meins F Jr. 1997. Silencing of transgenes introduced into leaves by agroinfiltration: a simple, rapid method for investigating sequence requirements for gene silencing. Molecular & General Genetics **256**, 581–585.

Shimada TL, Shimada T, Hara-Nishimura I. 2010. A rapid and non-destructive screenable marker, FAST, for identifying transformed seeds of *Arabidopsis thaliana*. The Plant Journal **61**, 519–528.

Shivhare D, Mueller-Cajar O. 2017. In vitro characterization of thermostable CAM Rubisco activase reveals a Rubisco interacting surface loop. Plant Physiology **174**, 1505–1516.

Simkin AJ, Lopez-Calcagno PE, Raines CA. 2019. Feeding the world: improving photosynthetic efficiency for sustainable crop production. Journal of Experimental Botany **70**, 1119–1140.

South PF, Cavanagh AP, Lopez-Calcagno PE, Raines CA, Ort DR. 2018. Optimizing photorespiration for improved crop productivity. Journal of Integrative Plant Biology **60**, 1217–1230.

Spreitzer RJ. 2003. Role of the small subunit in ribulose-1,5-bisphosphate carboxylase/oxygenase. Archives of Biochemistry and Biophysics **414**, 141–149.

Turkina MV, Blanco-Rivero A, Vainonen JP, Vener AV, Villarejo A. 2006. CO_2 limitation induces specific redox-dependent protein phosphorylation in *Chlamydomonas reinhardtii*. Proteomics **6**, 2693–2704.

van Nues RW, Beggs JD. 2001. Functional contacts with a range of splicing proteins suggest a central role for Brr2p in the dynamic control of the order of events in spliceosomes of *Saccharomyces cerevisiae*. Genetics **157**, 1451–1467.

Walter M, Chaban C, Schütze K, *et al*. 2004. Visualization of protein interactions in living plant cells using bimolecular fluorescence complementation. The Plant Journal **40**, 428–438.

Waltz E. 2017. Digital farming attracts cash to agtech startups. Nature Biotechnology **35**, 397–398.

Wang H, Gau B, Slade WO, Juergens M, Li P, Hicks LM. 2014. The global phosphoproteome of *Chlamydomonas reinhardtii* reveals complex organellar phosphorylation in the flagella and thylakoid membrane. Molecular & Cellular Proteomics **13**, 2337–2353.

Wunder T, Cheng SLH, Lai SK, Li HY, Mueller-Cajar O. 2018. The phase separation underlying the pyrenoid-based microalgal Rubisco supercharger. Nature Communications **9**, 5076.

Yamano T, Sato E, Iguchi H, Fukuda Y, Fukuzawa H. 2015. Characterization of cooperative bicarbonate uptake into chloroplast stroma in the green alga *Chlamydomonas reinhardtii*. Proceedings of the National Academy of Sciences, USA **112**, 7315–7320.

Yin X, Struik PC. 2017. Can increased leaf photosynthesis be converted into higher crop mass production? A simulation study for rice using the crop model GECROS. Journal of Experimental Botany **68**, 2345–2360.

Yizhi Z, Hélène L, Antoine S, Régine L, Brigitte G. 2018. Exploring intrinsically disordered proteins in *Chlamydomonas reinhardtii*. Scientific Reports **8**, 6805.

Zhan Y, Marchand CH, Maes A, *et al*. 2018. Pyrenoid functions revealed by proteomics in *Chlamydomonas reinhardtii*. PLoS One **13**, e0185039.

Zimmermann L, Stephens A, Nam SZ, Rau D, Kübler J, Lozajic M, Gabler F, Söding J, Lupas AN, Alva V. 2018. A completely reimplemented MPI bioinformatics toolkit with a new HHpred server at its core. Journal of Molecular Biology **430**, 2237–2243.